

Molecular-Dynamics Simulation of a Methane–Oxygen Mixture: Prediction of *P–V–T* Data and Evaluation of Effective Pair Potential Models

Naser Seyed Matin* and Amir Hossein Jalili

National Iranian Oil Company (NIOC), Research Institute of Petroleum Industry (RIPI), Qom Road, P. O. Box 18745-4391, Tehran, Iran

Received April 6, 2005; E-mail: matinn@ripi.ir

The results of a molecular-dynamics simulation using various isotropic pair potential functions for pure methane, oxygen, and their binary mixtures in the temperature range of 200 to 600 K and densities up to about 1.5 times their critical density is presented. The models studied in this work were: 1) Lennard–Jones (12–6) potential functions with different parameters, which have been proposed for methane and oxygen in the literature, 2) various types of Mie(n–m) potential with different values of n and m, for both methane and oxygen molecules, and 3) a potential function introduced by Dymond, Rigby, and Smith (DRS model). A Kihara–Mie(20–6) potential with the best value for the Kihara parameter, "γ" and optimized σ and ε is proposed for an oxygen molecule. Considering the predicting capability of the mentioned potential functions for pure methane and oxygen, two of them were selected for investigating methane–oxygen binary mixtures. The CH_4–CH_4 and O_2–O_2 center-of-mass radial distribution function, calculated with selected potentials, predicts the positions and peak height for $g(r)_{CH_4-CH_4}$ and $g(r)_{O_2-O_2}$ in good agreement with experimental data. The Deiters equation of state was used for *PVT* data production of pure methane and oxygen and their mixtures via imposing an intuitive mixing rule for the equation-of-state parameters. The results show good agreement between the LJ(12–6) and DRS potential models and the Deiters equation of state at densities of up to 0.25 g mL^{-1} at all temperatures, the deviations increasing by increasing the density. Furthermore, in the case of a methane–oxygen binary mixture, the Peng–Robinson equation of state was applied. The results reveal a strong influence of the binary interaction parameter, $\bar{k}_{ij}$ over the predicting ability of the Peng–Robinson equation of state for the mixture under study.

Predicting the equilibrium properties of fluids is being considered as one of the active fields in scientific and technological research. Methane, being the major component of natural gas, is also a fluid with great attractions. Knowledge about the properties of pure methane and its mixtures in the molecular scale would enable one to predict the natural gas behavior, which is essential for the natural gas industries. A lack of sufficient experimental data in some cases is the driving force to deeply view fluids, such as methane and its mixtures, from a molecular standpoint. Understanding the molecular behavior of fluids enables one to simulate their properties under dangerous or rare conditions. Nowadays, molecular-dynamics (MD) simulations are widely used in the investigations of fluid properties, as a powerful branch of molecular simulation.[1,2] Enlightenment regarding the molecular forces is the key point to do this job. For systems with known pair potentials, MD simulations give the equilibrium and transport properties in an acceptable range of accuracy, and in some cases the results of such simulations can be considered as experimental data.[3]

Travis and Gubbins[4] modeled the oxygen molecule as a two-center Lennard–Jones (2C-LJ) molecule. Zasetsky and Svishchev[5] modeled oxygen as a Lennard–Jones diatomic molecule carrying three point charges, using the MD simulations of liquid oxygen in the temperature range from 84 to 120 K. Miyano[6] performed Monte–Carlo (MC) simulations on oxygen by using a site–site pair potential model together with a triplet potential.

Stassen[7] performed MD simulations for liquid methane, and obtained the equilibrium and dynamical properties of liquid methane for 13 different potential models at a temperature of 150 K and a density of 28 mol L^{-1}. By considering 11 different relative orientations of methane molecules, Rowley and Pakkanen[8] derived an analytical site–site potential model for use in MD simulations of methane from ab-initio calculations. Saager et al.[9] predicted *PVT* data for Ar, CH_4, O_2, C_2H_6, and C_2H_4 at densities of up to two-thirds of the critical density (ρ_c) and temperatures up to three-times the critical temperature (T_c). They used LJ and 2C-LJ potentials and tested the mentioned potentials for fluids in the gas region.

Knowledge of the equilibrium and transport properties of a methane–oxygen mixture in the supercritical region is of practical importance. This type mixture is used in fuel consumption systems (for example in combustion engines, rocket engines, or future airplane turbines) as well as in the OCM (oxidative coupling of methane) process.[10] Experimental and theoretical data about various properties of this mixture are, however, scarce. Liuti and Pirani[11] studied the interaction of atomic and molecular oxygen with methane through a molecular-beam technique. They chose a Simon–Parr–Finalan modification of the Dunham expansion (SPFD) as a potential model to fit the potential parameters. Excess and interaction second-virial coefficients (B_{12}) of this system were measured by

Published on the web December 9, 2005; DOI 10.1246/bcsj.78.2105

Table 1. Potential Energy and Parameters Used for MD Simulations of Methane

Model	Type	ε/k (K)	σ/Å	r_m/Å	Ref.
M1	LJ(12–6)	149.92	3.7327		16
M2	LJ(12–6)	148.2	3.817		17
M3	Mie(20–6)	217	3.56		19
M4	Mie(28–7)	308.8	3.359		20
M5	Mie(14–7)	210.9	3.619		20
M6	DRS	181.6	3.69[a)]	4.268	18

a) The value of σ was obtained from equation $U_{\mathrm{DRS}}(\sigma) = 0$.

Table 2. Potential Energy and Parameters Used for MD Simulations of Oxygen

Model	Type	ε/k (K)	σ/Å	r_m/Å	Ref.
O1	LJ(12–6)	117.5	3.58		17
O2	LJ(12–6)	115.7	3.535		20
O3[a)]	Mie(20–6)	170.3	3.324		This work
O4	Mie(14–7)	169.3	3.247		20
O5	DRS	143.8	3.38[b)]	3.909	18

a) The Kihara parameter "γ" for this potential was evaluated to be 0.02. b) The value of σ was obtained from equation $U_{\mathrm{DRS}}(\sigma) = 0$.

Martin et al.[12] in the temperature range 290–320 K by using the method of Knobler et al. There are also a few experimental data[13] for the binary diffusion coefficient (D_{12}) of CH_4–O_2. Bzowski et al.[14] calculated the equilibrium and transport properties of this as well as other systems at low density by means of an extended principle of corresponding states. Maghari and Jalili[15] calculated the transport coefficients of the CH_4–O_2 and CH_4–N_2 systems from the extended law of corresponding states for the viscosity and the experimental second-virial coefficient data by an iterative inversion method.

The aim of this work is to predict the equilibrium properties of pure methane and oxygen molecules and their binary mixture via MD simulations by using isotropic pair potential functions available in the literature. In addition, a new potential model of the Kihara–Mie(20–6) type is proposed for the oxygen molecule, the parameters of which are optimized by means of experimental second-virial coefficient data. In this way, the MD results for pure methane and oxygen are compared with the experimental *PVT* data. The radial distribution function for pure methane and oxygen are calculated for each potential model by a MD simulation. Obtaining the best potential model(s) for pure methane and oxygen systems enables us to choose the best one for their mixture. Because of the lack of experimental *PVT* data for the CH_4–O_2 binary mixture, the calculated *PVT* results from MD simulations in this work are compared with those predicted by the Deiters and Peng–Robinson EOSs. Also, the interaction second-virial coefficients for CH_4–O_2 were calculated by means of the selected potential models and compared with the experimental and calculated values available in the literature. The simulations were performed at temperatures of 200 to 600 K and densities of up to 1.5 times the critical densities for pure methane and oxygen. The temperature and density range for the methane–oxygen mixture were 200 to 600 K, and densities up to about 20 mol L^{-1}. The details of the simulations and a brief description of the potential models are given in the remainder of the article.

Potential Models

In this study, the interactions of methane and oxygen molecules were modeled by isotropic pair potentials. Three groups of potential-energy functions were used for MD simulations in this work, which included Lennard–Jones(12–6) (LJ),[16,17] Dymond–Rigby–Smith (DRS),[18] and Mie(n–m)[19,20] potentials. The functional form of the potential models is as follows:

$$U_{\mathrm{LJ}}(r_{ij}) = 4\varepsilon\left[\left(\frac{\sigma}{r_{ij}}\right)^{12} - \left(\frac{\sigma}{r_{ij}}\right)^{6}\right], \tag{1}$$

$$U_{\mathrm{DRS}}(r_{ij}) = \varepsilon\left[0.331\left(\frac{r_m}{r_{ij}}\right)^{28} - 1.2584\left(\frac{r_m}{r_{ij}}\right)^{24} + 2.07151\left(\frac{r_m}{r_{ij}}\right)^{18} - 1.74452\left(\frac{r_m}{r_{ij}}\right)^{8} - 0.39959\left(\frac{r_m}{r_{ij}}\right)^{6}\right], \tag{2}$$

$$U_{\mathrm{Mie}(n-m)}(r_{ij}) = \left(\frac{n}{n-m}\right)\left(\frac{n}{m}\right)^{m/(n-m)}\varepsilon\left[\left(\frac{\sigma}{r_{ij}}\right)^{n} - \left(\frac{\sigma}{r_{ij}}\right)^{m}\right], \tag{3}$$

where r_m of Eq. 2 is the intermolecular separation at the minimum energy, ε, σ is the effective diameter, and n and m of Eq. 3 are the potential exponents, which take integer values. Tables 1 and 2 show a list of potential-energy functions and their parameters employed for the MD simulations of methane and oxygen in this study.

Using experimental data for the second-virial coefficient of oxygen,[21] the parameters of the Kihara–Mie(20–6) potential (the value of $n = 20$ for this model was chosen in analogy with the Mie(20–6) potential for methane[19]) and the value for the dimensionless Kihara parameter, γ,[22] were optimized. The ε and σ values were obtained exactly in the same manner as described in the next section for the CH_4–O_2 system. Then, by varying the value of the γ parameter from zero to 1, and

computing the RMSD value for the calculated second-virial coefficients with respect to the experimental data in the entire temperature range, we could reach the optimum value of this parameter. Eventually, the obtained potential function (i.e. O3 in Table 2) is given by

$$U = 2.3933\varepsilon\left[\left(\frac{1-\gamma}{r^*-\gamma}\right)^{20} - \left(\frac{1-\gamma}{r^*-\gamma}\right)^{6}\right], \quad (4)$$

where $r^* = r/\sigma$ and the best value for the Kihara parameter was acquired to be $\gamma = 0.02$, with the minimum root mean square deviation (RMSD) defined by

$$\mathrm{RMSD} = \sqrt{\frac{\sum_i (P_{i_{\mathrm{calcd}}} - P_{i_{\mathrm{exp.}}})^2}{N}}, \quad (5)$$

for the experimental second-virial coefficient data of pure oxygen. The same approach was applied for methane, but the results show negative values for γ, which are unacceptable.

Computational Details

The MD simulations were performed with different potential energy functions introduced in the previous section over systems consisting of 256 particles. Three-dimensional periodic boundary conditions and minimum image criteria were applied in all simulations, without Verlet's neighbor list. The temperature was kept constant by imposing momentum scaling for the translational motion. The particles in the simulation box were initially arranged in an fcc lattice. Generally, each of the equilibrium and production runs was performed in 100000 time steps. The time step was chosen to be 0.0006 in units of $\sigma(m/\varepsilon)^{1/2}$. A fifth-order predictor-corrector scheme[23] was applied to numerically integrate the equations of motion. Long-range corrections were accomplished with a shifted force potential for the pressure and potential according to Haile.[3] The cutoff distance for shifting the potential was chosen to be half of the box length. All units are defined in the usual reduced form. Table 3 lists the units used in our MD simulations.

MD simulations were carried out at densities and temperatures in the range of $0 < \rho \leq 1.5\rho_c$ and $200 \leq T \leq 600$ K, respectively, and the pressures and radial distribution functions (RDFs) were calculated in the usual manner.[24]

Results and Discussion

Pure Methane and Oxygen. The calculated pressures for pure methane and oxygen with the different potential models studied in this work and their experimental values are given in Tables 4 and 5, respectively. The RMSD of each potential in predicting the pressure compared to its corresponding experimental values is given in the last rows of Tables 4 and 5. The semi-empirical EOS derived by Deiters[25] was used to compare the simulation results, particularly for the mixture under study (see appendix). Baonza et al.[26] concluded that Deiters EOS gives good predictions for vapor–liquid equilibrium as well as the second-virial coefficients for those substances with the critical compressibility factor, Z_c, included in the interval $0.210 \leq Z_c \leq 0.291$, methane and oxygen being located in the upper boundary limit of this region. Therefore, for the sake of comparing the simulation results, we considered the Deiters EOS. The last columns in Tables 4 and 5 display the calculated pressures by means of Deiters EOS.

A comparison of RMSD for different potentials reveals that Kihara–Mie(20–6) with optimized parameters in this work and the DRS potential models (i.e. O3 and O5 in Table 2, respectively) give a good prediction of the oxygen equilibrium pressure compared with other potential models.

In the case of methane, the DRS and LJ models (i.e. M1 and M6 in Table 1, respectively) show the lowest values of RMSD. The drawback of the DRS potential is its computational time, which is nearly three-times that of the other Mie(n–m)-type potentials. The procedure that was employed to optimize the potential parameters of the CH_4–O_2 mixture in this work will be discussed in the following paragraphs.

Figure 1 shows the CH_4–CH_4 center of mass (COM) radial distribution function (RDF) calculated in this work by different

Table 3. Reduced Units Used in the MD Simulations

Quantity	Reduced units
Density	$\rho^* = \rho\sigma^3$
Temperature	$T^* = k_B T/\varepsilon$
Time	$t^* = (\varepsilon/m\sigma^2)^{1/2}t$
Length of the simulation box	$L^* = L/\sigma$

Table 4. Comparison of *PVT* Data from MD Simulations with Experimental Results and the Deiters EOS for Methane[a)]

No.	T/K	d/mol L^{-1}	P_{exp} (Ref. 32)[b)]	P(M1)[b),c)]	P(M2)[b),c)]	P(M3)[b),c)]	P(M4)[b),c)]	P(M5)[b),c)]	P(M6)[b),c)]	P_{Deiters}[b)]
1	200.00	12.000	6.35	6.56(0.30)	6.45(0.26)	3.84(0.38)	1.46(1.17)	4.19(0.64)	5.91(0.56)	6.59
2	206.00	21.022	33.80	37.75(0.82)	54.75(0.55)	3.17(1.13)	3.87(2.24)[d)]	16.24(2.03)	33.05(0.75)	33.95
3	250.00	18.000	36.32	38.58(0.40)	45.18(0.75)	19.68(0.84)	12.78(1.36)	22.17(0.86)	35.97(1.40)	37.64
4	290.00	18.000	54.29	55.81(0.93)	65.23(0.38)	37.22(1.17)	27.80(1.57)	45.48(0.75)	53.44(1.01)	56.45
5	300.00	17.000	50.48	52.75(0.60)	60.92(0.93)	37.79(0.90)	25.20(0.79)	38.81(1.03)	50.99(1.35)	52.64
6	320.00	17.000	58.24	58.82(0.75)	66.67(1.15)	45.36(1.34)	34.66(1.16)	50.30(0.57)	57.17(1.04)	60.80
7	448.20	7.000	27.12	27.26(0.37)	27.84(0.39)	26.21(0.19)	27.06(0.29)	27.06(0.29)	27.14(0.15)	27.20
8	500.00	18.000	142.49	145.64(1.29)	161.91(0.73)	123.33(0.93)	101.16(1.41)	128.44(1.07)	143.48(1.49)	153.81
9	598.29	7.000	39.71	39.96(0.23)	40.95(0.28)	36.07(0.23)	38.05(0.31)	39.11(0.31)	39.81(0.23)	40.05
	No. of steps/CPU sec			66	66	66	60	60	21	
	RMSD:			1.33	6.67	9.31	14.94	6.39	0.80	2.36

a) $T_c = 190.564$ K, $\rho_c = 10.139$ mol L^{-1}, $P_c = 4.5992$ MPa, nbp $= 111.667$ K. b) All pressures are in MPa. c) The values in the parenthesis show the corresponding standard deviations. d) Negative pressure.

Table 5. Comparison of Pressures from MD Simulations with Experimental Results and the Deiters EOS for Oxygen[a)]

No.	T/K	d/mol L^{-1}	P_{exp} (Refs. 30 and 31)[b)]	P(O1)[b),c)]	P(O2)[b),c)]	P(O3)[b),c),d)]	P(O3)[b),c),e)]	P(O4)[b),c)]	P(O5)[b),c)]	$P_{Deiters}$[b)]
1	200.00	17.000	18.27	24.10(0.66)	22.33(0.37)	13.23(1.16)	15.92(0.57)	16.34(0.35)	17.85(0.38)	18.47
2	250.00	18.000	36.32	44.32(0.49)	42.88(0.40)	32.18(0.62)	34.74(0.64)	32.06(0.53)	35.82(0.79)	36.35
3	290.00	18.000	49.33	60.80(0.38)	59.61(0.40)	50.27(1.10)	50.25(1.18)	41.86(0.97)	48.57(0.64)	49.32
4	300.00	18.000	52.56	62.20(0.58)	60.88(0.56)	53.38(0.45)	53.04(0.62)	47.98(0.76)	53.34(0.60)	52.55
5	320.00	18.000	58.98	71.81(0.59)	68.76(0.50)	58.78(0.44)	61.28(0.89)	54.48(0.65)	59.48(0.96)	59.03
6	400.00	17.465	80.00	95.36(1.38)	90.46(0.41)	79.45(0.87)	79.40(0.88)	73.44(0.66)	81.10(0.45)	80.40
7	500.00	14.371	80.00	88.91(0.48)	87.24(0.48)	80.04(1.14)	80.77(0.99)	76.52(0.53)	82.28(0.55)	80.01
8	600.00	12.251	80.00	86.09(0.46)	85.41(0.57)	80.48(0.65)	81.59(0.66)	77.49(0.55)	82.39(0.71)	79.83
No. of steps/CPU sec				66	66	60	60	66	21	
RMSD:				6.90	5.54	1.84	1.08	3.32	1.16	0.34

a) $T_c = 154.581$ K, $\rho_c = 13.63$ mol L^{-1}, $P_c = 5.0430$ MPa, nbp $= 90.1878$ K. b) All pressures are in MPa. c) The values in the parenthesis show the corresponding standard deviations. d) Kihara–Mie(20–6) potential with $\gamma = 0$. e) Kihara–Mie(20–6) potential with $\gamma = 0.02$.

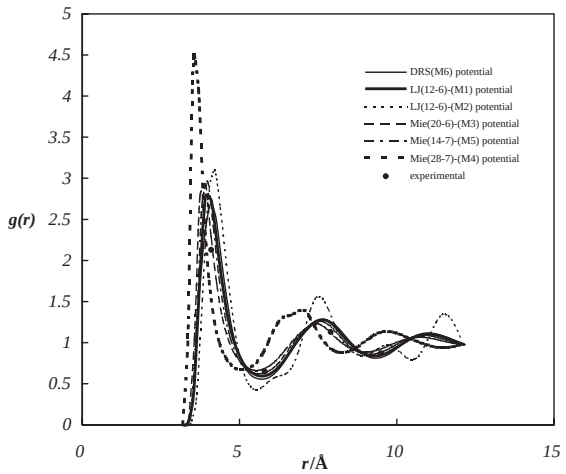

Fig. 1. Radial distribution function for the COM–COM pair correlations in liquid methane at 150 K and 28 mol L^{-1}.

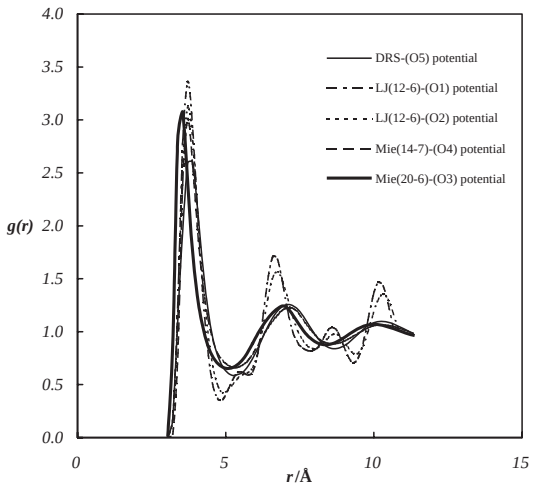

Fig. 2. Radial distribution function for the COM–COM pair correlations in liquid oxygen at 100 K and 34.1 mol L^{-1}.

potentials compared with the experimental data from Ref. 7. Figure 2 also displays the center-of-mass RDF calculated in this work for O_2–O_2 compared with the results given in Ref. 5. Tables 6 and 7 show the peak positions and peak heights of the calculated center of mass (COM) RDF in this study and their experimental values for methane and oxygen, respectively.[5,7] As it can be seen that both selected potentials predict the same value for the peak positions and the peak heights for $g(r)_{CH_4-CH_4}$ and $g(r)_{O_2-O_2}$, which are in a good agreement with experimental data.

Methane–Oxygen Mixture. Using the optimum potential models obtained in the previous section for pure O_2 and CH_4, mixtures of these systems were investigated in this work. As can be deduced from Tables 4 and 5, the DRS potential predicts the *PVT* experimental data for O_2 and CH_4 fairly well. The LJ(12–6) potential proposed by Saager and Fischer[16] can also predict the *PVT* properties of methane with a good degree of accuracy. In this investigation, two types of potential models, i.e. DRS and LJ(12–6), were used for the MD simulations of methane–oxygen binary mixtures. In the first group of simulations, all of the similar and dissimilar interactions were modeled by the DRS potential function. In the second group, the LJ(12–6) potential was used to describe all the interactions. Model O2 (Table 2) was employed for O_2–O_2, and model M1 (Table 1) for CH_4–CH_4 interactions. Although the Kihara–Mie(20–6) potential model proposed in this work has a good ability for predicting the *PVT* properties of oxygen, nevertheless for the sake of simplicity and convenience, the LJ(12–6) model was also employed for the methane–oxygen mixture. Two approaches were taken to optimize the cross-potential parameters (CH_4–O_2 parameters) of this mixture. In the first approach, using only the Lorentz–Berthelot (LB) combining rule, the potential parameters for the CH_4–O_2 mixture were determined by pure component parameters:[24]

$$\sigma_{ij} = (\sigma_{ii} + \sigma_{jj})/2, \tag{6}$$

$$\varepsilon_{ij} = (\varepsilon_{ii}\varepsilon_{jj})^{1/2}. \tag{7}$$

In the second approach, the potential parameters obtained by the Lorentz–Berthelot combining rule were considered as the initial estimate for further investigations. Then, the better estimation for the mixture was calculated through experimental data for the second-virial coefficients. The second-virial coefficient can be written in a reduced form,

Table 6. Maxima and Minima Positions (First Number in A) and Heights (Second Number) of the COM–COM Pair Distribution Function $g_{CC}(r)$ of Liquid Methane for the Investigated Potential Models

Model	1st max	1st min	2nd max	2nd min	3rd max
M1	3.9/2.78	5.8/0.60	7.7/1.28	9.3/0.84	11.0/1.10
M2	4.2/3.10	5.5/0.43	7.4/1.55	9.0/0.84	9.7/0.97
M3	3.9/2.93	5.5/0.66	7.5/1.23	9.1/0.88	10.9/1.07
M4	3.5/4.46	5.0/0.67	7.1/1.39	8.2/0.87	9.7/1.13
M5	4.0/2.96	5.6/0.62	7.6/1.26	9.2/0.86	10.9/1.09
M6	4.1/2.68	5.7/0.55	7.6/1.28	9.4/0.81	11.0/1.13
Exp. (Ref. 6)	4.1/2.13	5.8/0.65	7.9/1.13	9.5/0.87	—

Table 7. Maxima and Minima Positions (First Number in A) and Heights (Second Number) of the COM–COM Pair Distribution Function $g_{CC}(r)$ of Liquid Oxygen for the Investigated Potential Models

Model	1st max	1st min	2nd max	2nd min	3rd max
O1	3.9/3.36	5.2/0.36	7.0/1.71	8.4/0.82	9.1/1.04
O2	3.9/3.13	5.1/0.43	7.1/1.57	8.3/0.84	9.0/0.97
O3	3.7/3.08	5.2/0.65	7.0/1.24	8.5/0.88	10.0/1.07
O4	3.6/3.01	5.2/0.66	6.8/1.23	8.3/0.89	9.9/1.06
O5	3.9/2.60	5.3/0.59	7.1/1.26	8.6/0.84	10.3/1.10
Ref. 20	3.8/2.65	5.2/0.50	6.8/1.32	8.5/0.86	9.9/1.00

$$B_{12}{}^{*} = -3\int_0^{\infty}(e^{-u^*/T^*} - 1)r^{*2}\mathrm{d}r^{*}, \tag{8}$$

where, $T^* = KT/\varepsilon$, $r^* = r/\sigma$ and

$$B_{12} = \frac{2\pi N_A \sigma_{12}^3}{3} B_{12}{}^{*}. \tag{9}$$

The distance at which $U(r) = 0$, or σ, can be determined by means of the experimental second-virial coefficients and Eq. 9 through an iterative method for each potential function. For this purpose, 1) the initial values of the potential parameters, including σ and ε of pure oxygen and methane, are adopted from the literature. 2) By applying the LB combining rule, the initial values of σ and ε for the mixture are estimated. 3) Mixtures' $B_{12}{}^{*}$ are calculated from Eq. 8 for each temperature. 4) σ is determined by linear regression using Eq. 9 for B_{12}. 5) The obtained value for σ is selected for calculating a new set of $B_{12}{}^{*}$ with the initially chosen ε. Step 4 is then repeated for calculating a new σ. This process (i.e. steps 4 and 5) is applied repeatedly until the optimized σ with minimum RMSD for the second-virial coefficients at different temperatures is achieved. In this procedure, only the value for σ is optimized and the initial value calculated from the LB combining rule is kept constant in the course of the iteration for ε. Finally, having obtained σ, the value of ε is tuned near its initial value, so that the results for second-virial coefficients can be improved. While the number of experimental data points for the second-virial coefficient for a mixture of CH_4–O_2 is scarce,[12] the results of the above-mentioned iterative procedure for determining σ reveal that this approach has been proven to be useful for the desired purposes. Table 8 gives the optimized parameters for the best potentials (DRS and LJ) for the CH_4–O_2 system, and Table 9 gives the values of the second-virial coefficient obtained by means of the two approaches cited above for the CH_4–O_2 mixture. The results in Table 9 show that the DRS and LJ(12–6) potential models with optimized parameters can be regarded as the best choice for MD simulations of the CH_4–O_2 mixture.

Table 8. Best Potential Functions with Their Optimized Parameters for the CH_4–O_2 System, Proposed in This Work

Model	Type	ε/k (K)	σ/Å	r_m/Å
DRS-mix	DRS	155.8	3.478	4.0224
LJ-mix	LJ(12–6)	126.8	3.621	

Figure 3 and Table 10 show the variation of the experimental second-virial coefficient as a function of temperature for the CH_4–O_2 system in comparison with the results obtained from different potential energy functions, the Deiters EOS and the corresponding state principle introduced by Bzowski et al.[14] As Figure 3 reveals at high temperatures, as the sign of the

Table 9. Second-Virial Coefficients Obtained by Potential Models with Optimized Parameters in This Work Mixture and also A Simple LB Combining Rule for CH_4–O_2

T/K	B_{12}(exp)[a)]	B_{12}(DRS)-LB[b)]	DRS-mix[c)]	B_{12}(LJ)-LB[b)]	LJ-mix[c)]
290	−25.7	−30.09	−25.59	−29.08	−25.59
300	−22.7	−27.09	−22.87	−26.2	−22.88
320	−18.1	−21.77	−18.04	−21.06	−18.04

a) Data from Ref. 12. b) LB: Lorentz–Berthelot combining rule. c) mix: This work.

second-virial coefficient changes, discrepancy in the results obtained from different approaches appears. The Deiters EOS produces larger second-virial coefficients at high temperatures. This can be argued based on the derivation of the Deiters EOS. The square-well potential model for fluids produced this equation. The results obtained in this work for binary mixtures of CH_4–O_2 with different compositions give a simple mixing rule to calculate the mixture parameters from the pure component parameters in the Deiters EOS.[26] It can be concluded that between the potentials investigated in this study, because of good consistency at high temperature region with other calculated values, the LJ(12–6) is the best potential with the proposed optimized parameters in this work. Thus, we chose this potential for MD simulations of the CH_4–O_2 mixture.

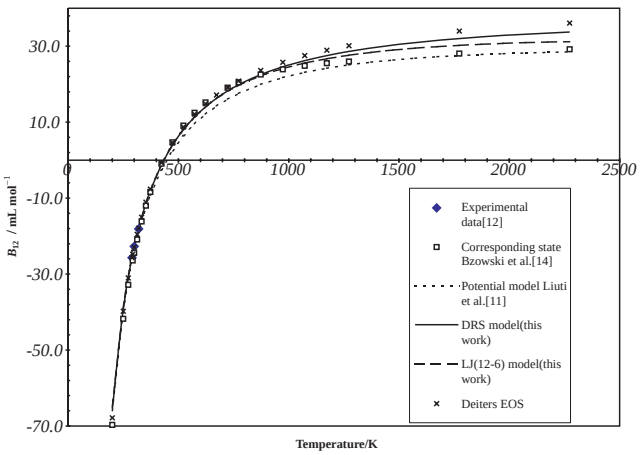

Fig. 3. Comparison of B_{12} values for CH_4–O_2 of this work with the others.

Regarding the three adjustable parameters of this EOS (see appendix, Eqs. A·12–A·14), the following mixing rule can be offered intuitively, at least for binary mixtures for Deiters EOS:

$$\ln a_m = x_1 \ln a_1 + x_2 \ln a_2, \tag{10}$$

$$b_m = (x_1 {b_1}^{1/3} + x_2 {b_2}^{1/3})^3, \tag{11}$$

$$\ln c_m = x_1 \ln c_1 + x_2 \ln c_2. \tag{12}$$

The above equations can be obtained by taking the natural logarithm of both sides of Eqs. A·12 and A·14, and then by replacing the 1/2 coefficient by the mole fraction (x_i) of each component. In order to test Eqs. 10–12, two different compositions of CH_4–O_2 mixture were studied in addition to an equimolar system. As can be seen from Table 11, the results confirm the proposed mixing rule. Of course, an improved and more accurate mixing rule is proposed for the Deiters EOS by the authors (a manuscript is under preparation).

Besides the Deiters EOS, the well-known Peng–Robinson (PR) EOS[27] was also used for comparison of the MD results considered in this work. Figures 4–6 display isotherms calculated for an equimolar CH_4–O_2 mixture with the Deiters and PR EOSs, virial equation of state truncated after the second-virial coefficient and MD simulations with selected potentials for the CH_4–O_2 mixture. The second-virial coefficients applied in a truncated virial equation of state were the experimental

Table 10. Comparison of the Interaction Second-Virial Coefficients for the Methane–Oxygen System

T/K	B_{12}(exp)[12]	B_{12}(Bzowski)[14]	B_{12}(Liuti)[11]	B_{12}(Deiters)[25]	B_{12}(DRS)[a)]	B_{12}(LJ)[b)]
200.00		−69.72	−65.94	−67.83	−65.47	−64.90
250.00		−41.76	−39.76	−39.77	−39.05	−38.99
273.15		−32.84	−31.48	−31.00	−30.69	−30.68
290.00	−25.70		−26.44	−25.71	−25.59	−25.59
293.15		−26.40	−25.57	−24.76	−24.71	−24.71
300.00	−22.70	−24.43	−23.76	−22.90	−22.87	−22.88
313.15		−20.90	−20.54	−19.52	−19.62	−19.62
320.00	−18.10		−18.99	−17.90	−18.04	−18.04
333.15		−16.15	−16.22	−15.00	−15.23	−15.22
353.15		−11.99	−12.47	−11.08	−11.42	−11.39
373.15		−8.35	−9.19	−7.65	−8.07	−8.02
423.15		−0.93	−2.54	−0.71	−1.26	−1.18
473.15		4.71	2.50	4.58	3.93	4.03
523.15		9.07	6.44	8.74	8.02	8.11
573.15		12.48	9.58	12.10	11.32	11.39
623.15		15.19	12.14	14.87	14.03	14.06
723.15		19.09	16.04	19.15	18.22	18.13
773.15		20.50	17.54	20.85	19.86	19.70
873.15		22.56	19.94	23.61	22.53	22.21
973.15		23.90	21.74	25.77	24.59	24.11
1073.15		24.84	23.13	27.51	26.22	25.57
1173.15		25.50	24.23	28.93	27.54	26.72
1273.15		25.96	25.10	30.12	28.63	27.64
1773.15		28.05	27.55	33.99	32.03	30.22
2273.15		29.18	28.49	36.11	33.74	31.22

a) DRS potential model: $\varepsilon_{12}/k = 155.8\,\mathrm{K}$, $\sigma_{12} = 3.478\,\text{Å}$, $r_{m12} = 4.0224\,\text{Å}$. b) LJ(12–6) potential model: $\varepsilon_{12}/k = 126.8\,\mathrm{K}$, $\sigma_{12} = 3.621\,\text{Å}$.

Table 11. Comparison of the Calculated Pressure for CH_4–O_2 Mixture by MD Simulation, Virial, and Deiters EOSs at $T = 290\,K$, $\rho = 0.100\,g\,mL^{-1}$

Methane mole fraction	$P_{2nd.vir}$[a] (MPa)	P_{MD}[b] (MPa)	$P_{Deiters}$[c] (MPa)
0.25	7.92	8.05	7.93
0.75	9.84	10.71	10.25

a) Calculated pressure through experimental second-virial coefficients. $B_{mix} = x_1^2 B_{11} + 2x_1x_2B_{12} + x_2^2B_{22}$. b) Calculated pressure through molecular-dynamic simulation. c) Calculated pressure through Deiters equation using Eqs. 10–12 for EOS parameters.

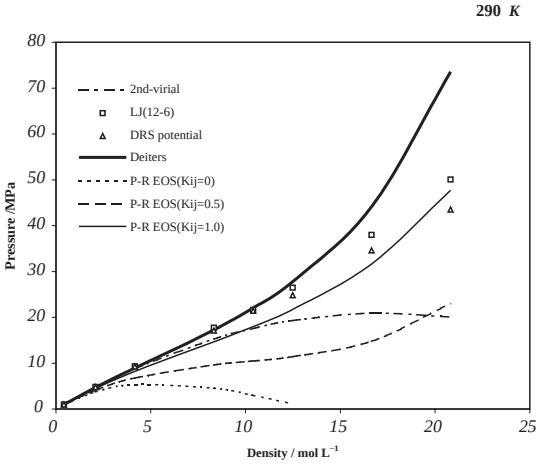

Fig. 4. The P–ρ isotherm for equimolar mixture of CH_4–O_2 at 290 K.

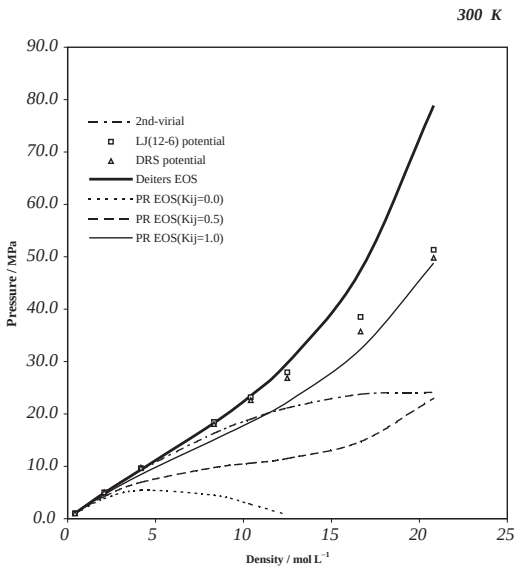

Fig. 5. The P–ρ isotherm for equimolar mixture of CH_4–O_2 at 300 K.

data from Ref. 12. Considering the MD simulation results as criteria, it can be revealed from Figs. 4–6 that the Deiters EOS predict *PVT* data up to a density of $0.25\,g\,mL^{-1}$ fairly

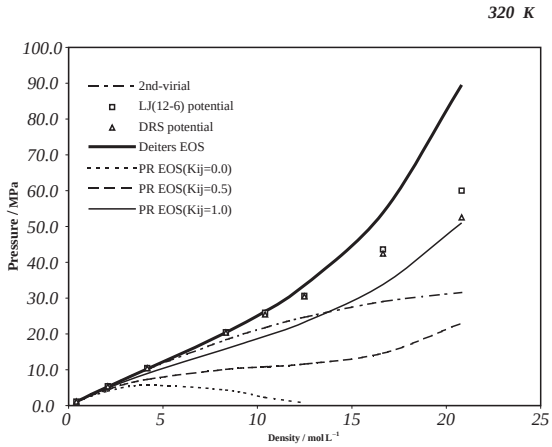

Fig. 6. The P–ρ isotherm for equimolar mixture of CH_4–O_2 at 320 K.

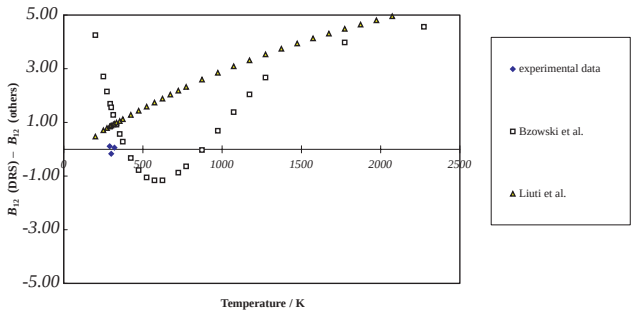

Fig. 7. Deviation plots for second-virial coefficient of CH_4–O_2 calculated by the DRS potential function.

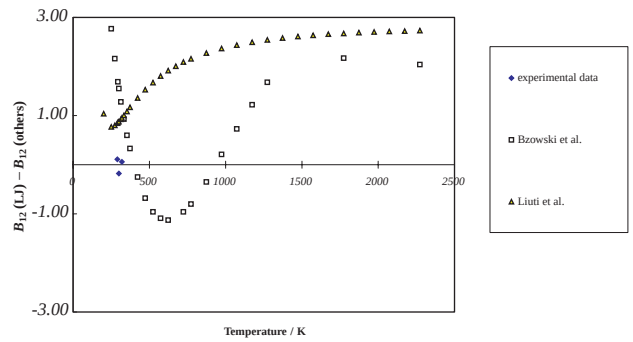

Fig. 8. Deviation plots for second-virial coefficient of CH_4–O_2 calculated by the LJ(12–6) potential function.

well. For the PR EOS, the following mixing rule was implemented,[27]

$$a_m = \sum_i \sum_j x_i x_j (a_i a_j)^{1/2} (1 - \bar{k}_{ij}), \quad (13)$$

$$b_m = \sum_i x_i b_i, \quad (14)$$

where x_i is the mole fraction of component i and $\bar{k}_{ij}$ is the temperature-dependent binary interaction parameter. As can be seen from Figs. 4–6, depending on the $\bar{k}_{ij}$ values applied for the PR EOS, different trends are observed. It seems that the prediction of the PR EOS becomes better as the value of the

binary interaction coefficient approaches unity.

Figures 7 and 8 show deviation plots for B_{12} calculated by DRS and LJ(12–6) for the methane–oxygen binary mixture. As can be seen from Fig. 7, the DRS potential prediction shows a remarkable deviation at high temperature, which increases as the temperature goes up. This can be argued for an applicable temperature range of the DRS potential, which is 200 up to 500 K.[18]

Conclusion

Different isotropic potential functions were investigated for the CH_4, O_2, and CH_4–O_2 systems. For the sake of simplicity, these systems were considered to be as simple as spherical molecules. Therefore, the molecular directions made no difference for the applied pair potential in this study. Afterwards, Kihara–Mie(20–6) with the best value for the Kihara parameter, $\gamma = 0.02$ and optimized $\sigma = 3.324$ Å, $\varepsilon/k = 170.3$ K and DRS[18] (models O3 and O5, respectively) were proposed for the oxygen molecule.

In the case of pure methane DRS[18] and LJ(12–6)[16] potentials (models M6 and M1, respectively) gave good predictions for equilibrium pressures.

For the mixture CH_4–O_2, this study set forth that a new parameterized DRS potential function with parameters $\sigma = 3.478$ Å, $\varepsilon/k = 155.8$ K, and $r_m = 4.0224$ Å, and LJ(12–6) potential function with $\sigma = 3.621$ Å, $\varepsilon/k = 126.8$ K are the best simple potentials for predicting the CH_4–O_2 mixture equilibrium properties. Since the potential function parameters for the CH_4–O_2 mixture were determined, the calculated second-virial coefficients with these potential functions show good agreement with the experimental data. Deiters introduced mixing rules for his equation, which are applicable over a wide range of densities.[28,29] Considering the Lorentz–Berthelot combining rule for potential function parameters, the intuitive simple mixing rule for binary mixture parameters in the Deiters equation of state was proposed and used in this work.

List of Symbols. a, b, and c: Equation of state parameters, k: Boltzmann constant, ln: natural logarithm, m: mass, N: number of experimental data point in Eq. 5, P: pressure, R: gas constant, r: intermolecular distance, T: temperature, V_m: molar volume, x: mole fraction, Z_c: critical compressibility factor.

Greek Letters. ε: Potential well depth, σ: the distance at which $U(r) = 0$, γ: Kihara potential model parameter, ρ: density.

This research was fully supported by the National Iranian Oil Company (NIOC) Research Institute of Petroleum Industry (RIPI).

Appendix

Eq. A·1 gives Deiters equation of state,[25]

$$P = \frac{RT}{V_m}\left(1 + cc_0\frac{4\eta - 2\eta^2}{(1-\eta)^3}\right) - \frac{abR\tilde{T}_{\text{eff}}}{{V_m}^2}(\exp(1/\tilde{T}_{\text{eff}}) - I)I_1(\tilde{\rho}). \quad \text{(A·1)}$$

The equation has three adjustable parameters (a, b, and c), which are the characteristic temperature, covolume, and shape factor, respectively.

$$\eta = (\pi/6)\sigma^3 N_A/V_m, \quad \text{(A·2)}$$

$$\tilde{\rho} = b/V_m, \quad \text{(A·3)}$$

$$\tilde{T} = cT/a, \quad \text{(A·4)}$$

$$\tilde{T}_{\text{eff}} = (\tilde{T} + \lambda\tilde{\rho})/y. \quad \text{(A·5)}$$

Here, η is the packing fraction, $\lambda = -0.06911c$ is a parameter that introduces three-body effects into the equation of state, $c_0 = 0.6887$.

$$I_1(\tilde{\rho}) = \left(\frac{\gamma}{c}\right)^2 \sum_0^5 (i+1)h_i\gamma^i\tilde{\rho}^i, \quad \text{(A·6)}$$

where $h_0 = 7.0794046$, $h_1 = 12.08351455$, $h_2 = -53.6059$, $h_3 = 143.6681$, $h_4 = -181.1554682$, $h_5 = 78.5739255$.

$$\gamma = 1 - 0.697816(c-1)^2. \quad \text{(A·7)}$$

$$y(\tilde{\rho}) = f^2 - c^{-5.5}f(1-f) + (1 - 0.65/c)(1-f)^2, \quad \text{(A·8)}$$

where the relative free volume is

$$f = \exp(cc_0(3\eta^2 - 4\eta)/(1-\eta)^2). \quad \text{(A·9)}$$

The adjustable parameters (a and b) are related to square-well potential parameters,

$$a = \varepsilon/k_B, \quad \text{(A·10)}$$

$$b = N_A\sigma^3/2^{1/2}. \quad \text{(A·11)}$$

Using the Lorentz–Berthelot combining rule for the pair potential parameters, the following combination rule was derived for adjustable parameters for equimolar binary mixtures:

$$a_{12} = \frac{\varepsilon_{12}}{k} = \frac{(\varepsilon_1\varepsilon_2)^{1/2}}{k} = \left(\frac{\varepsilon_1}{k}\right)^{1/2}\left(\frac{\varepsilon_2}{k}\right)^{1/2} = (a_1a_2)^{1/2}, \quad \text{(A·12)}$$

$$b_{12} = \frac{N_A{\sigma_{12}}^3}{\sqrt{2}} = \frac{N_A}{\sqrt{2}}\left[\frac{1}{2}(\sigma_1 + \sigma_2)\right]^3 = \frac{N_A}{8\sqrt{2}}(\sigma_1 + \sigma_2)^3 = \left[\frac{1}{2}({b_1}^{1/3} + {b_2}^{1/3})\right]^3, \quad \text{(A·13)}$$

$$c_{12} = \frac{a_{12}\tilde{T}}{T} = \frac{(a_1a_2)^{1/2}\tilde{T}}{T} = \left(\frac{a_1\tilde{T}}{T}\right)^{1/2}\left(\frac{a_2\tilde{T}}{T}\right)^{1/2} = (c_1c_2)^{1/2}. \quad \text{(A·14)}$$

References

1 B. C. Attwood and C. K. Hall, *Fluid Phase Equilib.*, **204**, 85 (2003).

2 P. S. Crozier and R. L. Rowley, *Fluid Phase Equilib.*, **193**, 53 (2002).

3 J. M. Haile, "Molecular Dynamics Simulation: Elementary Methods," John Wiley & Sons, Inc. (1992).

4 K. P. Travis and K. E. Gubbins, *Langmuir*, **15**, 6050 (1999).

5 A. Y. Zasetsky and I. M. Svishchev, *Chem. Phys. Lett.*, **334**, 107 (2001).

6 Y. Miyano, *Fluid Phase Equilib.*, **104**, 71 (1995).

7 H. Stassen, *J. Mol. Struct.: THEOCHEM*, **464**, 107 (1999).

8 R. L. Rowley and T. Pakkanen, *J. Chem. Phys.*, **110**, 3368 (1999).

9 B. Saager, A. Lotfi, M. Bohn, V. N. Nguyen, and J. Fischer, *Fluid Phase Equilib.*, **54**, 237 (1990).

10 "Methane and Alkane Conversion Chemistry," ed by D. W. Slocum and M. D. Bhasin, Plenum Press, New York (1996).

11 G. Liuti and F. Pirani, *J. Chem. Phys.*, **87**, 5266 (1987).
12 M. L. Martin, R. D. Trengove, K. R. Harris, and P. J. Dunlop, *Aust. J. Chem.*, **35**, 1525 (1982).
13 R. E. Walker and A. A. Westenberg, *J. Chem. Phys.*, **32**, 436 (1960).
14 J. Bzowski, J. Kestin, E. A. Mason, and F. J. Uribe, *J. Phys. Chem. Ref. Data*, **19**, 1179 (1990).
15 A. Maghari and A. H. Jalili, *J. Phys. Soc. Jpn.*, **73**, 1191 (2004).
16 B. Saager and J. Fischer, *Fluid Phase Equilib.*, **57**, 35 (1990).
17 J. O. Hirschfelder, C. F. Curtiss, and R. B. Bird, "Molecular Theory of Gases and Liquids," Wiley, New York (1964).
18 J. H. Dymond, M. Rigby, and E. B. Smith, *J. Chem. Phys.*, **42**, 2801 (1965).
19 G. P. Matthews and E. B. Smith, *Mol. Phys.*, **32**, 1719 (1976).
20 M. Edalat, S. S. Lan, F. Pang, and G. A. Mansoori, *Int. J. Thermophys.*, **1**, 177 (1980).
21 J. H. Dymond and E. B. Smith, "The Virial Coefficients of Pure Gases and Mixtures," Clarendon Press, Oxford (1980).
22 J. A. Barker, W. Fock, and F. Smith, *Phys. Fluids*, **7**, 897 (1964).
23 C. W. Gear, "Numerical Initial Value Problems in Ordinary Differential Equations," Prentice Hall, Englewood Cliffs (1971).
24 M. P. Allen and D. J. Tildesley, "Computer Simulation of Liquids," Clarendon Press, Oxford (1987).
25 U. Deiters, *Chem. Eng. Sci.*, **36**, 1139 (1981).
26 V. G. Baonza, M. Caceres, and J. Nunez, *Fluid Phase Equilib.*, **78**, 43 (1992).
27 R. C. Reid, J. M. Prausnitz, and B. E. Poling, "The Properties of Gases and Liquids," 4th ed, McGraw-Hill (1987).
28 U. K. Deiters, *Fluid Phase Equilib.*, **33**, 267 (1987).
29 H. J. R. Guedes, J. A. Zollweg, E. J. M. Filipe, L. F. G. Martins, and J. C. G. Calado, *J. Chem. Thermodyn.*, **34**, 669 (2002).
30 R. Schmidt and W. Wagner, *Fluid Phase Equilib.*, **19**, 175 (1985).
31 B. A. Younglove, *J. Phys. Chem. Ref. Data*, **11**, 1 (1982).
32 B. A. Younglove and J. F. Ely, *J. Phys. Chem. Ref. Data*, **16**, 577 (1987).